Applied Physics Letters ARTICLE scitation.org/journal/apl

Conformal gradient-index phononic crystal lens for ultrasonic wave focusing in pipe-like structures

Cite as: Appl. Phys. Lett. **117**, 021906 (2020); doi: 10.1063/5.0012316
Submitted: 30 April 2020 · Accepted: 6 July 2020 ·
Published Online: 16 July 2020

Hrishikesh Danawe,[1] Gorkem Okudan,[2] Didem Ozevin,[2] and Serife Tol[1,a)]

AFFILIATIONS

[1]Department of Mechanical Engineering, University of Michigan, Ann Arbor, Michigan 48109, USA
[2]Civil and Materials Engineering, University of Illinois at Chicago, Chicago, Illinois 60607, USA

[a)]Author to whom correspondence should be addressed: stol@umich.edu

ABSTRACT

We explore a conformal gradient-index phononic crystal lens integrated within a pipe to amplify guided wave modes toward improved ultrasonic inspection of pipelines. The proposed conformal lens is composed of an array of cylindrical steel stubs attached to the outer surface of a steel pipe, which are tailored according to the hyperbolic secant profile of refractive index in the circumferential direction of the pipe. Hence, the ultrasonic guided wave energy is focused in the axial direction of the pipe and amplified at the focal point of the lens. Refractive indices are calculated using dispersion curves obtained from the finite element simulations of the stubbed unit cells, and the curved lens is designed for the second longitudinal wave mode of the pipe, which is commonly used in guided wave testing. The proposed lens design is implemented on a steel pipe, which is typically used in the distribution networks utilized in cities, and simultaneous focusing of longitudinal wave modes in a broad frequency range is verified through both numerical models and experimental measurements.

Guided wave ultrasonics is widely used for non-destructive evaluation and structural health monitoring of civil infrastructures including pipelines, bridges, and rail tracks that require accelerated inspection and repair.[1] In the last decade, the assessment of pipeline integrity has been studied using guided wave ultrasonics because of its ease of operation, low cost, and high sensitivity to detect the early state of structural defects.[2] In guided wave testing, various ultrasonic wave modes could be triggered and utilized for understanding the structural integrity. The ultrasonic wave in the pipe-like structures mainly propagates in two directions: circumferential and axial. Specifically, the wave in the axial direction involves the longitudinal waves and torsional waves. In addition, the flexural mode may exist due to non-axisymmetric motion of the particles. The mode and frequency selection associated with the pipe geometry influence the ability of guided wave propagation over long distances which is critical for long-range damage inspection.[3,4] While researchers have intensively studied techniques to excite multi-order longitudinal,[5] flexural,[6] and torsional[7] wave modes in pipelines, improving the quality of receiver signal carrying defect information at the other end is relatively less explored. Specifically, attenuation and scattering of guided waves traveling through a long-range pipeline result in weak signals retrieved at sensor locations, which limits the range and scale of damage detection. To overcome this limitation, multichannel transducer phase arrays have been studied and utilized to focus elastic waves at defect locations.[8,9] The phased array technology is knowledge based and requires the angular profile database of guided waves for the underlying algorithm to accurately evaluate the input signal parameters of each transducer channel in order to achieve focusing at desired locations. In this paper, we propose a broadband gradient-index phononic crystal (GRIN-PC) lens-based wave focusing technique to amplify the signal energy at the positions of the receiving sensors enabling the transmission of damage information over long distances.

In recent years, phononic crystals and metamaterials have attracted increasing attention due to their ability to manipulate and control the propagation of elastic waves in ways that are not possible in conventional materials.[10] These artificially engineered periodic structures have unique properties such as bandgaps and the ability to slow the velocity of waves;[11,12] hence, they offer the potential for a variety of applications including vibration and noise attenuation,[13] frequency filtering,[14] cloaking,[15,16] sensing,[17] and energy harvesting,[18–20] among others. In addition to these applications, GRIN lenses designed by engineering the dispersion curves offer an effective method to localize elastic wave energy.[20] For instance, they have been integrated with piezoelectric energy harvesters, which resulted in a significant increase in the harvested power output.[18] Similarly, refractive gradient-index concepts based on tailoring wave propagation characteristics can also

benefit guided wave ultrasonics by properly focusing the wave energy at sensor locations.[21] Inspired by gradient-index optics, Lin *et al.*[22] designed the first GRIN-PC lens with solid cylinders embedded in an epoxy medium such that the refractive index along the direction transverse to the phononic wave propagation had a hyperbolic secant (HS) gradient distribution. Hence, the incident bulk waves were bent gradually toward the center axis where the refractive index was the highest (or the wave speed was the lowest), resulting in convergence at a focal spot. To date, GRIN lenses have been implemented in planar structures in both macro-[18–20,22] and micro-scales.[23,24] However, GRIN-based focusing concepts in non-planar structures have not been fully explored yet. In this paper, we implement GRIN theory in pipe-like structures to amplify ultrasonic wave signal at the focal points (FPs) of the lens (at sensor locations) for improved sensing toward enhancing guided wave ultrasonics. To this end, broadband focusing of the longitudinal wave modes, namely, L(0, 1) and L(0, 2) pipe modes, which are commonly used in ultrasonic inspection of pipelines, is studied through numerical models and validated with experiments.

The proposed conformal GRIN-PC lens design is composed of an array of curved unit cells formed by cylindrical steel stubs attached to the outer surface of a 4-in. profile steel pipe [inner diameter (*ID*) of 102.3 mm and outer diameter (*OD*) of 114.3 mm] as shown in Fig. 1(a). The lattice constant (a) is determined as 20 mm considering their conformal distribution on the pipe surface, and the stub heights are tailored according to the hyperbolic secant profile of refractive index in circumferential direction of the pipe to gradually bend the guided wave energy toward the centerline of the lens. The lens is 13-unit-cells wide in the circumferential direction covering more than 80% of the circumference. Wave propagation characteristics of the lattice structure are obtained by performing eigenfrequency analysis of the unit cell in COMSOL Multiphysics by applying Floquet periodicity boundary conditions across its sides and sweeping the wavenumber along the edges of the first Irreducible Brillouin Zone. Two longitudinal wave modes, namely, L(0, 1) and L(0, 2) pipe modes, are identified in the band structure and dispersion plots of the unit cells with varying stub heights (h_s) as shown in Figs. 1(b) and 1(c), and the corresponding mode shapes are depicted in Fig. 1(a). The numbers 1 and 2 in the nomenclature of L(0, 1) and L(0, 2) wave modes represent the implicit family orders of the guided waves generated in pipe with the given wall thickness (t_p) and frequency range.[25] Both these modes are axisymmetric with zero circumferential order represented by the first index of their names. The dominant particle displacement for L(0, 1) wave mode is radially outward resulting in uniform sinusoidal bulging out and caving in of the pipe, whereas the dominant particle displacement for L(0, 2) wave mode is in the direction of wave propagation resulting in sinusoidal axial compression and rarefaction of the pipe.[26] Using the dispersion information, we can obtain the relationship between the stub height variation of the two dimensional lattice and the refractive index n, which is defined for a particular wave mode at certain frequency as[22]

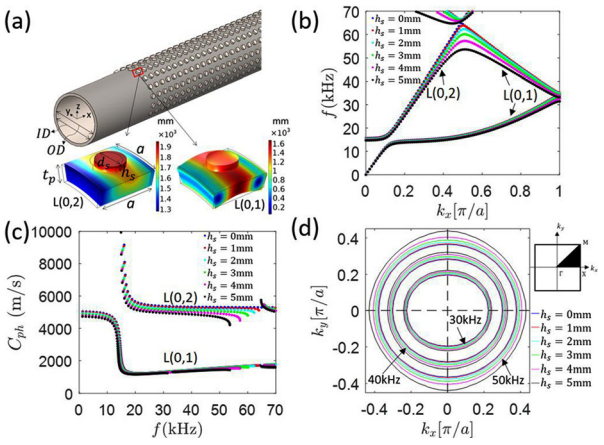

FIG. 1. (a) Conformal GRIN lens design and mode shapes of the unit cell at 50 kHz. (b) Band structure and (c) dispersion curves of L(0, 2) and L(0, 1) modes of unit cell with varying stub heights. (d) Equal frequency contours for L(0, 2) mode at 30 kHz, 40 kHz, and 50 kHz.

$$n = \frac{1}{2}\left(\frac{\upsilon}{\upsilon_{\Gamma X}} + \frac{\upsilon}{\upsilon_{\Gamma M}}\right) = \frac{1}{2}\left(\frac{\upsilon}{\omega/k_{\Gamma X}} + \frac{\upsilon}{\omega/k_{\Gamma M}}\right), \tag{1}$$

where $\upsilon_{\Gamma X}$ and $\upsilon_{\Gamma M}$ are phase velocities and $k_{\Gamma X}$ and $k_{\Gamma M}$ are wave numbers of a wave mode in phononic crystal along ΓX and ΓM symmetry directions, respectively, and υ is the reference phase velocity of that wave mode in plain pipe at angular frequency ω. From the dispersion diagram, it is observed that the phase velocity of a particular mode at certain frequency decreases and refractive index increases with increased stub height. Considering the highest variation in the phase velocity and avoiding the bandgap formation around 53 kHz, we set the limit for design frequency as 50 kHz and target focusing guided wave energy above the audible range (above 20 kHz) as commonly used in ultrasonic testing. Figure 1(d) presents the equal frequency contours, which are obtained by finding the dispersion curves for all wave vectors within the first Brillouin zone of the lattice and plotting the contour of wave vectors that correspond to equal frequencies. The contours reveal the nature of the lattice with circular contours meaning that the lattice is isotropic having equal wave speeds along all directions. Note that, for small anisotropy at 50 kHz as verified with equal frequency contour plot in Fig. 1(d), refractive index calculation is based on the phase velocity along ΓX, which is the predominant direction of wave propagation. While at lower frequencies, the equal frequency contours show anisotropy, and thus phase velocity along all symmetry directions is considered for evaluating effective refractive index as defined by Eq. (1). The conformal GRIN lens is designed by tailoring stub heights according to the dispersion curve variation of the L(0, 2) mode at 50 kHz based on the hyperbolic secant (HS) profile of the refractive index,

$$n(s) = n_0\,\mathrm{sech}(\alpha s), \tag{2}$$

where n_0 is the refractive index of the curved lattice located at the centerline of the lens, α is the gradient coefficient, and s is circumferential location of stubs in terms of lattice constant, a. For the curved lens with a 13-cell-wide aperture size, the optimal stub heights are obtained as (4.5000, 4.4646, 4.3188, 4.0668, 3.6588, 2.9682, and 1.9158) mm at locations $s = [0, \pm a, \pm 2a, \pm 3a, \pm 4a, \pm 5a, \pm 6a]$ such that the highest stub with the highest refractive index (lowest phase speed) is located at the centerline as illustrated in Fig. 2(a). As a result, when the guided wave is incident upon the GRIN lens, it will be gradually bent toward the center axis, and wave energy is concentrated at a focal spot. GRIN theory[27] predicts the first focal point (FP) of a GRIN medium

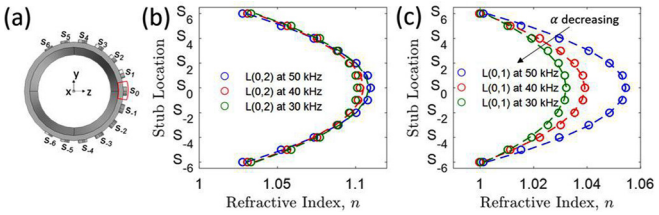

FIG. 2. (a) Curved lens design showing stub height profile around the pipe circumference. (b) Refractive index profiles (circles) for L(0, 2) and (c) L(0, 1) pipe modes at 30 kHz, 40 kHz, and 50 kHz with hyperbolic secant (HS) profile fits (dashed lines).

with HS distribution of refractive index at $\pi/2\alpha$. According to the HS profile of the L(0, 2) mode designed at 50 kHz as presented in Fig. 2(b), the gradient coefficient is determined as $\alpha = 0.064/a$ resulting in the first focal point of the L(0, 2) mode in the curved GRIN lens at $24.54a$. Hence, the dimension of the conformal lens in the propagation direction is finalized with $50a$ length. In addition, we theoretically explore the broadband focusing of the L(0, 2) pipe mode by exploiting its dispersion variation at lower frequencies. Figure 2(b) shows the refractive index distributions of the stubbed unit cells of the GRIN lens calculated at 40 kHz and 30 kHz and the best HS profiles fitted to those distributions. It is noteworthy to mention that due to the non-ideal redistribution of the refractive indices, it is impossible to obtain a HS profile fitting to all of the refractive indices of the unit cells. According to our analysis, which will be further discussed in the numerical simulations, it is found that fitting the refractive index values toward the edges is more critical than fitting the refractive index values at the center of the lens in terms of estimating the focal point. Hence, the best fit HS curves are ensured to satisfy refractive indices at $\pm 3a, \pm 4a, \pm 5a, \pm 6a$. Accordingly, the gradient coefficients are obtained as $\alpha = 0.061/a$ for 40 kHz and $\alpha = 0.062/a$ for 30 kHz yielding the first focal point predictions at $25.75a$ and $25.33a$, respectively. Furthermore, in addition to broadband amplification of the L(0, 2) pipe mode, we also investigate focusing of L(0, 1) pipe mode which has lower wave speed compared to L(0, 2) mode but still exhibits dispersion variation among different stub heights used in the GRIN design. Figure 2(c) shows the distribution of the refractive indices of the GRIN unit cells calculated for L(0, 1) pipe mode at 50 kHz, 40 kHz, and 30 kHz and the corresponding best fit HS curves. From the best fit HS profiles, the gradient coefficients are obtained as $\alpha = 0.055/a$, $\alpha = 0.046/a$, and $\alpha = 0.041/a$, and the focal distances are predicted at $28.56a$, $34.15a$, and $38.31a$ for L(0, 1) mode focusing at 50 kHz, 40 kHz, and 30 kHz, respectively. Hence, within the single lens design, we can theoretically achieve simultaneous amplification of both wave modes in a broad frequency range, which is first verified with numerical simulations.

The finite element model of the half-symmetric pipe is built in COMSOL Multiphysics using second-order tetrahedral mesh elements with 10 nodes per element. The maximum mesh size is set to satisfy 12 mesh elements per the smallest wavelength (i.e., $\lambda_{L(0,1)} = 29.3$ mm) with minimum element size set to $(1/5)$ th of the maximum size and a Courant–Friedrichs–Lewy number of 0.2 is selected to set the time step so that the wave is equally resolved in space resulting in the optimal solution. Low reflecting boundary conditions are applied at the pipe ends to avoid reflected waves interfering in the lens region. In addition to low reflecting boundary conditions applied at the pipe boundaries, the pipe length is ensured to prevent the wave interference due to boundary reflections. Longitudinal modes of the pipe [L(0, 1) and L(0, 2)] are excited using 24 equally spaced circular piezoelectric actuators (PZT-4)[5] that are modeled at the end of the pipe as shown in Fig. 3(a). The minimum number of transducers required for suppressing higher order flexural modes and exciting only the two axisymmetric longitudinal modes [L(0, 1) and L(0, 2)] can be determined from the relation provided by Rose.[28] The described piezoelectric actuator configuration only excites L(0, 1) and L(0, 2) pipe modes, which is confirmed by taking two-dimensional Fast Fourier Transform (2D FFT) of the wave field response and comparing it with theoretical dispersion curves of the steel pipe. In order to verify broadband performance of the lens, the actuator array is applied a seven-cycle sine burst voltage input with a Gaussian pulse window at multiple center frequencies of 30 kHz, 40 kHz, 50 kHz, and 65 kHz. From time-dependent simulations performed on the plain pipe, the velocity field response is extracted in the radial direction for L(0, 1) mode and in the axial direction for L(0, 2) mode and used as the baseline data. Then, the pipe model integrated with GRIN lens extending from $0a$ to $50a$ is numerically tested at the aforementioned frequencies. Figure 3(b) shows the instantaneous velocity fields from COMSOL Multiphysics simulations at the designed frequency (i.e., 50 kHz) where the focusing of both wave modes is clearly observed at different instances due to the difference in their phase speeds. The plane wave modes traveling along the GRIN lens bend toward the centerline of the lens and localize around the predicted focal spots. The peak wave energy densities are obtained from the normalized RMS wave fields calculated by integrating the L(0, 1) and L(0, 2) wave velocity fields over time at multiple frequencies as shown in Figs. 3(c) and 3(d) and compared with the theoretical focal distance predictions. Accordingly, the peak points are identified at $27a$ for L(0, 2) and at $36a$ for L(0, 1) modes at 50 kHz resulting in deviations from theoretical focal positions only 8% and 22%, respectively. Since the L(0, 1) pipe mode has more dispersive nature compared to the L(0, 2) pipe

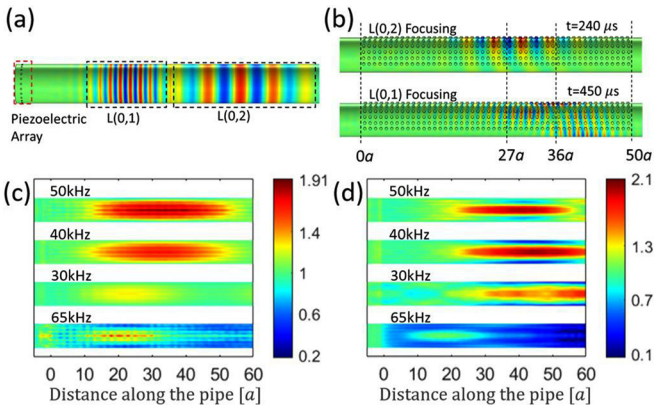

FIG. 3. (a) Generation of L(0, 2) and L(0, 1) pipe modes in the plain pipe by 24 equally spaced circular piezoelectric actuators. (b) Instantaneous velocity fields at 50 kHz showing focusing of L(0, 2) and L(0, 1) modes (side view of the pipe). (c) Normalized RMS axial velocity field showing broadband focusing of L(0, 2) mode (top view). (d) Normalized RMS radial velocity field (top view) showing broadband focusing of the L(0, 1) mode.

mode [Fig. 1(c)], the deviation from the theoretical focal point estimation is higher compared to the L(0, 2) pipe mode. Still the predicted focal point lies in the focusing neck of L(0, 1) mode which is narrow because of its smaller wavelength. On the other hand, wave energy of the L(0, 2) mode is distributed over a larger area near focal spot because of its larger wavelength. Near the focal spots of L(0, 2) and L(0, 1) modes, the maximum signal amplification factor at 50 kHz reaches 1.917 and 1.876, respectively. From the RMS wave fields at 40 kHz, the peak energy density is obtained at 32*a* and 46*a* with amplification factors of 1.708 and 1.913 for the L(0, 2) and L(0, 1) modes, respectively. As expected, focal point shifts away for both wave modes due to the decrease in the gradient coefficient as shown in Figs. 2(b) and 2(c) and the L(0, 2) mode prediction is in better agreement with the theory, while the discrepancy is larger for L(0, 1) mode. On the other hand at 30 kHz, the effect of redistribution of the refractive indices and non-ideal HS fit is more pronounced resulting in a large discrepancy between the theoretical predictions and numerical results. In addition, the difference can also be attributed to anisotropic behavior of the unit cells at lower frequencies. Unlike the trend in FPs shifting away at lower frequencies, the focal distance of the L(0, 2) mode decreases at 30 kHz, which proves the pronounced effect of refractive indices toward the edges of the lens as shown in Fig. 2(b). Note that the effect of the L(0, 1) mode bandgap about 32 kHz is visible in the wave field as the Gaussian pulse excitation creates waves propagating at the center frequency with 20 kHz bandwidth. Furthermore, we numerically test the lens at a higher frequency to better explore the bandgap effect and to illustrate an extreme case above the design frequency. Wave field simulations at 65 kHz show that the wave energy of both modes reduces in the lens region because of bandgap frequency as seen from the dispersion band structures presented in Figs. 1(b) and 1(c); hence, there is no significant propagation in the GRIN lens. Since the lens design is originally based on L(0, 2) wave mode at the designed frequency of 50 kHz, larger deviation from the theoretical FPs is expected for L(0, 1) mode and for lower frequencies because of the non-ideal HS distribution of the refractive indices as shown in Figs. 2(b) and 2(c) along with the other factors discussed here. Also, applying narrow bandwidth signals by increasing the number of cycles in the sine burst excitation would yield a better agreement with the numerical and the theoretical predictions of GRIN theory, which considers a single design frequency. However, there are practical limitations in increasing the signal length as it would result in boundary reflections interfering in the lens region. Still, we can conclude that the proposed conformal lens focuses multiple wave modes in a broad range of frequencies as verified with the numerical models presented in Figs. 3(c) and 3(d).

In the experimental validation of the proposed lens, we utilize a 152 cm long prototype steel pipe with a 4-in. profile which is the typical dimensions for the gas distribution pipes. Figure 4(a) shows the experimental setup with the GRIN-PC lens fabricated by gluing of the steel stubs with varying heights and the 24-equally spaced transducer arrangement around the pipe. The array of identical piezoelectric disks with 5 mm diameter and 0.4 mm thickness manufactured by Steminc is excited with a seven-cycle sine burst signal in a range of frequencies (20 kHz–100 kHz). Hence, the ultrasonic guided waves [L(0, 1) and L(0, 2) pipe modes] are simultaneously generated. Three individual piezoelectric disks attached at the predicted focal points function as receiving sensors. Each receiver is connected to a 40 dB gain

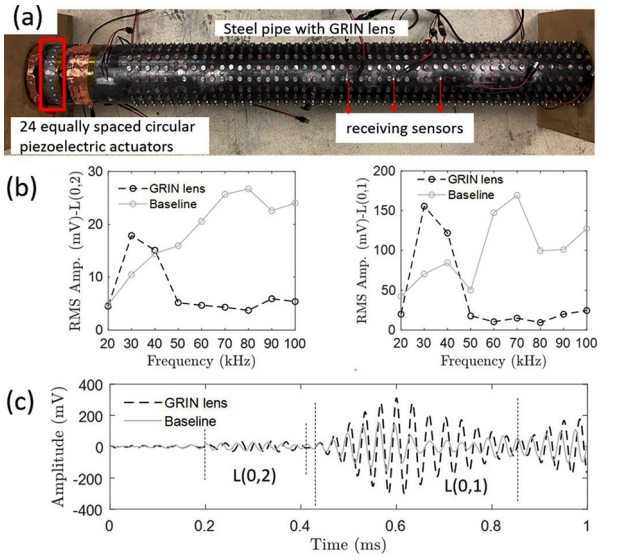

FIG. 4. (a) Experimental setup of the GRIN lens integrated steel pipe with the actuator array and receiving sensors at 25*a*, 30*a*, and 35*a* in the focal region of the lens. (b) Broadband amplification of L(0, 2) and L(0, 1) pipe modes measured at 25*a* and 30*a*, respectively. (c) Time signals measured at 30 kHz verifying simultaneous focusing of L(0, 2) and L(0, 1) modes propagating in the GRIN lens.

pre-amplifier and the PCI-8 data acquisition system manufactured by MISTRAS. The experiments are carried out for both the GRIN lens-integrated pipe and for the plain pipe as the baseline.

Figure 4(b) shows the amplification of the signal at the receiving points where the highest amplification is achieved for 30 kHz as presented with the time history presented in Fig. 4(c). Note that the measured signal is analyzed for the first arrival of wave modes at receiving sensors as depicted in Fig. 4(c). Hence, boundary reflections are avoided as consistent with the numerical model. According to the experimental results, the L(0, 2) mode is amplified by 1.71 times while the L(0, 1) mode is amplified by 2.21 times in the GRIN lens as compared to the baseline. However, at 50 kHz, the waveforms at the focal points significantly reduce in the pipe integrated with GRIN lens. Further investigation of the finite element models reveals that the dispersion curves of the unit cell modeled with a glue layer drop and exhibit a bandgap formation about 50 kHz. Hence, the significant reduction in signal amplitude at 50 kHz is attributed to the bandgap caused by the elastic effect of the glue layer used for bonding the stubs on the pipe surface. Consequently, the experimental results at 50 kHz corresponds to numerical results at 65 kHz [where the effect of the bandgap is clearly visible as shown in Figs. 3(b) and 3(c)], while the best focusing performance of the experimental GRIN lens shifts to a lower frequency (30 kHz) for both longitudinal modes. In addition, the manufacturing tolerances, the thin layer of paint on the pipe, possible misalignment of the stubs, and imperfect bonding are among the other factors causing discrepancy between the numerical and experimental results. Yet, because of the broadband capability of the proposed conformal lens, simultaneous focusing of the longitudinal wave modes is achieved and validated in a broad frequency range.

In summary, we have designed, fabricated, and numerically and experimentally validated a conformal GRIN-PC lens to amplify

ultrasonic guided waves in pipes. The non-planar lens is composed of curved unit cells with a hyperbolic secant distribution of refractive index to focus the wave energy transmitted by ultrasonic wave modes, namely L(0, 1) and L(0, 2) pipe modes commonly used in guided wave testing. Through computations and experimental measurements, it is demonstrated that both wave modes can be simultaneously focused within the same lens design in a broad range of frequencies. Despite imperfections in the experimental setup, we have shown general agreement between finite element models and measurements, verifying our design concept. Through wave field focusing in the broadband GRIN lens, multiple ultrasonic wave modes can propagate and transmit the damage-related information longer distances. Beyond pipelines, the proposed conformal lens concept can be extended to other pipe-like structures such as wind turbine blades, girders, and foundations. In addition to structural health monitoring applications, conformal lenses are also promising in other engineering applications like ultrasonic imaging and energy harvesting.

This work was supported by the National Science Foundation under Grant No. CMMI-1914583/1914663.

DATA AVAILABILITY

The data that support the findings of this study are available from the corresponding author upon reasonable request.

REFERENCES

[1]M. Mitra and S. Gopalakrishnan, "Guided wave based structural health monitoring: A review," Smart Mater. Struct. **25**, 053001 (2016).
[2]M. Lowe, D. Alleyne, and P. Cawley, "Defect detection in pipes using guided waves," Ultrasonics **36**, 147–154 (1998).
[3]H. Shin and J. Rose, "Guided wave tuning principles for defect detection in tubing," J. Nondestruct. Eval. **17**, 27–36 (1998).
[4]D. Alleyne and P. Cawley, "The excitation of lamb waves in pipes using dry-coupled piezoelectric transducers," J. Nondestruct. Eval. **15**, 11–20 (1996).
[5]P. Lowe, R. Sanderson, S. Pedram, N. Boulgouris, and P. Mudge, "Inspection of pipelines using the first longitudinal guided wave mode," Phys. Procedia **70**, 338–342 (2015).
[6]L. Tang and B. Wu, "Excitation mechanism of flexural-guided wave modes F(1, 2) and F(1, 3) in pipes," J. Nondestruct. Eval. **36**, 59 (2017).
[7]X. Niu, W. Duan, H.-P. Chen, and H. Marques, "Excitation and propagation of torsional T(0,1) mode for guided wave testing of pipeline integrity," Measurement **131**, 341–348 (2019).
[8]W. Luo and J. L. Rose, "Phased array focusing with guided waves in a viscoelastic coated hollow cylinder," J. Acoust. Soc. Am. **121**, 1945–1955 (2007).
[9]J. Li and J. L. Rose, "Angular-profile tuning of guided waves in hollow cylinders using a circumferential phased array," IEEE Trans. Ultrason., Ferroelectr., Freq. Control **49**, 1720–1729 (2002).
[10]Y. Jin, B. Djafari-Rouhani, and D. Torrent, "Gradient index phononic crystals and metamaterials," Nanophotonics **8**, 685–701 (2019).
[11]P. A. E. Deymier, *Acoustic Metamaterials and Phononic Crystals* (Springer Science and Business Media, 2013), Vol. 173.
[12]V. Laude, *Phononic Crystals: Artificial Crystals for Sonic, Acoustic, and Elastic Waves* (Walter de Gruyter GmbH and Co KG, 2015), Vol. 26.
[13]R. Martinez-Sala, J. Sancho, J. Sánchez-Pérez, V. Gomez, J. Llinares, and F. Meseguer, "Sound attenuation by sculpture," Nature **378**, 241 (1995).
[14]C. J. Rupp, M. L. Dunn, and K. Maute, "Switchable phononic wave filtering, guiding, harvesting, and actuating in polarization-patterned piezoelectric solids," Appl. Phys. Lett. **96**, 111902 (2010).
[15]S. A. Cummer and D. Schurig, "One path to acoustic cloaking," New J. Phys. **9**, 45–45 (2007).
[16]M. Farhat, S. Guenneau, and S. Enoch, "Ultrabroadband elastic cloaking in thin plates," Phys. Rev. Lett. **103**, 024301 (2009).
[17]Y. Chen, H. Liu, M. Reilly, H. Bae, and M. Yu, "Enhanced acoustic sensing through wave compression and pressure amplification in anisotropic metamaterials," Nat. Commun. **5**, 5247 (2014).
[18]S. Tol, F. L. Degertekin, and A. Erturk, "Gradient-index phononic crystal lens-based enhancement of elastic wave energy harvesting," Appl. Phys. Lett. **109**, 063902 (2016).
[19]S. Tol, F. L. Degertekin, and A. Erturk, "Phononic crystal Luneburg lens for omnidirectional elastic wave focusing and energy harvesting," Appl. Phys. Lett. **111**, 013503 (2017).
[20]J. Hyun, W. Choi, and M. Kim, "Gradient-index phononic crystals for highly dense flexural energy harvesting," Appl. Phys. Lett. **115**, 173901 (2019).
[21]H. Danawe, G. Okudan, D. Ozevin, and S. Tol, "Metamaterial-based amplification of multi-mode ultrasonic guided waves toward improved damage detection in pipelines," Proc. SPIE **11376**, 160–166 (2020).
[22]S.-C. S. Lin, T. J. Huang, J.-H. Sun, and T.-T. Wu, "Gradient-index phononic crystals," Phys. Rev. B **79**, 094302 (2009).
[23]T.-T. Wu, Y.-T. Chen, J.-H. Sun, S.-C. Lin, and T. Huang, "Focusing of the lowest antisymmetric lamb wave in a gradient-index phononic crystal plate," Appl. Phys. Lett. **98**, 171911 (2011).
[24]J. Zhao, R. Marchal, B. Bonello, and O. Boyko, "Efficient focalization of antisymmetric lamb waves in gradient-index phononic crystal plates," Appl. Phys. Lett. **101**, 261905 (2012).
[25]D. Ozevin and H. Yalcinkaya, "New leak localization approach in pipelines using single-point measurement," J. Pipeline Syst. Eng. Pract. **5**, 04013020 (2014).
[26]P. S. Lowe, H. Lais, V. Paruchuri, and T.-H. Gan, "Application of ultrasonic guided waves for inspection of high density polyethylene pipe systems," Sensors **20**, 3184 (2020).
[27]M. V. P. C. Gómez-Reino and C. Bao, *Gradient-Index Optics: Fundamentals and Applications* (Springer, Berlin, 2002).
[28]J. L. Rose, *Ultrasonic Guided Waves in Solid Media* (Cambridge University Press, 2014).